DOI: 10.1021/ic901636f

Inorganic Chemistry
Article

Actinide Redox-Active Ligand Complexes: Reversible Intramolecular Electron-Transfer in U(dpp-BIAN)$_2$/U(dpp-BIAN)$_2$(THF)

Eric J. Schelter, Ruilian Wu, Brian L. Scott, Joe D. Thompson, Thibault Cantat, Kevin D. John, Enrique R. Batista, David E. Morris, and Jaqueline L. Kiplinger*

Los Alamos National Laboratory, Los Alamos, New Mexico 87545

Received August 14, 2009

Actinide complexes of the redox-active ligand (dpp-BIAN)$^{2-}$ (dpp-BIAN = 1,2-bis(2,6-diisopropylphenylimino)acenaphthylene), U(dpp-BIAN)$_2$ (**1**), U(dpp-BIAN)$_2$(THF) (**1-THF**), and Th(dpp-BIAN)$_2$(THF) (**2-THF**), have been prepared. Solid-state magnetic and single-crystal X-ray data for complex **1** indicate a ground-state $U^{IV}-\pi^{*4}$ configuration, whereas a (dpp-BIAN)$^{2-}$-to-uranium electron transfer occurs for **1-THF**, resulting in a $U^{III}-\pi^{*3}$ ground configuration. The solid-state magnetic data also indicate that interconversion between the two forms of the complex is possible, limited only by the ability of tetrahydrofuran (THF) vapor to penetrate the solid upon cooling of the sample. In contrast to those in the solid state, spectroscopic data acquired in THF indicate only the presence of the $U^{IV}-\pi^{*4}$ form for **1-THF** in solution, evidenced by electronic absorption spectra and by measurement of the solution magnetic moment in THF-d_8 using the Evans method. Also reported is the electrochemistry of the complexes collected in CH_2Cl_2, $CF_3C_6H_5$, and THF. As expected from the solution spectroscopic data, only small differences are observed in half-wave potentials of ligand-based processes in the presence of THF, consistent with the solution $U^{IV}-\pi^{*4}$ configuration of the complexes in all cases. Density functional theory calculations were undertaken for complexes **1** and **1-THF** to determine if intrinsic energetic or structural factors underlie the observed charge-transfer process. While the calculated optimized geometries agree well with experimental results, it was not possible to arrive at a convergent solution for **1-THF** in the $U^{III}-\pi^{*3}$ configuration. However, perturbations in the orbital energies in **1** versus **1-THF** for the $U^{IV}-\pi^{*4}$ configuration do point to a diminished highest occupied molecular orbital−lowest unoccupied molecular orbital energy gap in **1-THF**, consistent with the solid-state magnetic data. These results represent the first example of a stable and well-defined, reversible intramolecular electron transfer in an actinide complex with redox-active ligands.

Introduction

Metal complexes possessing redox-active ligands constitute a rapidly growing area of interest in inorganic and organometallic chemistry.[1−4] Redox-active ligands display reversible redox changes between two or more stable oxidation states that introduce the possibility for electron-transfer processes between the metal ion and ligand.[5] The electronic structures of transition metal complexes exhibiting intramolecular electron transfer often display interesting phenomena including thermal, pressure, or photoinduced valence changes (i.e., valence tautomerism) as a consequence of their closely spaced electronic states.[6,7] In the context of their electronic properties, we have recently become interested in 5f-element complexes of redox-active ligands and how ligand "noninnocence" might manifest in these complexes in which the metal-orbital participation in bonding is often considerably smaller than that observed in transition metal complexes.

Reports of f-element complexes supported by classical redox-active ligands such as catecholates have appeared; however, the focus of these studies has generally been on their structural features rather than their physicochemical properties.[8−12] Considerably more effort has been devoted

*To whom correspondence should be addressed. E-mail: kiplinger@lanl.gov.

(1) Vasudevan, K.; Cowley, A. H. *Chem. Commun.* **2007**, 3464–3466.
(2) Blackmore, K. J.; Lal, N.; Ziller, J. W.; Heyduk, A. F. *J. Am. Chem. Soc.* **2008**, *130*, 2728–2729.
(3) Trovitch, R. J.; Lobkovsky, E.; Bill, E.; Chirik, P. J. *Organometallics* **2008**, *27*, 1470–1478.
(4) Lu, C. C.; Bill, E.; Weyhermueller, T.; Bothe, E.; Wieghardt, K. *J. Am. Chem. Soc.* **2008**, *130*, 3181–3197.
(5) Ray, K.; Petrenko, T.; Wieghardt, K.; Neese, F. *Dalton Trans.* **2007**, 1552–1566.
(6) Hendrickson, D. N.; Pierpont, C. G. *Top. Curr. Chem.* **2004**, *234*, 63–95.
(7) Sato, O.; Cui, A.; Matsuda, R.; Tao, J.; Hayami, S. *Acc. Chem. Res.* **2007**, *40*, 361–369.
(8) Xu, J.; Gorden, A. E. V.; Raymond, K. N. *Eur. J. Org. Chem.* **2004**, 3244–3253.
(9) Belkhiri, L.; Arliguie, T.; Thuery, P.; Fourmigue, M.; Boucekkine, A.; Ephritikhine, M. *Organometallics* **2006**, *25*, 2782–2795.
(10) Hitchcock, P. B.; Huang, Q.; Lappert, M. F.; Wei, X.-H.; Zhou, M. *Dalton Trans.* **2006**, 2991–2997.
(11) Weis, E. M.; Barnes, C. L.; Duval, P. B. *Inorg. Chem.* **2006**, *45*, 10126–10130.
(12) Zhu, D.; Kappel, M. J.; Raymond, K. N. *Inorg. Chim. Acta* **1988**, *147*, 115–121.

Published on Web 12/29/2009

to ytterbium diimine complexes, which present redox activity derived from the readily accessible Yb^{II}/Yb^{III} redox couple; Yb^{III} reduction in aqueous solution versus SHE is −1.15 V.[13−15] Recent reports have also included the observation of temperature-dependent redox isomerism in solution for a ytterbium dpp−BIAN complex.[16] In all cases, these electronic structure effects are ascribed to steric pressure in the ytterbium coordination sphere,[15] a clear manifestation of the sterically induced reduction concept developed by Evans.[17] Our work has also shown that energetically proximate charge-transfer electronic excited states, derived from intramolecular electron-transfer processes, mix with lower-lying f-orbital-based ligand-field states in uranium complexes, resulting in significant intensity enhancement of the f−f transitions.[18−24] In light of these observations, and of our interest in probing the effects of ligand redox activities when coordinated to f-element metal ions, we initiated an investigation of actinide complexes of the redox-active ligand, dpp-BIAN = 1,2-bis(2,6-diisopropylphenylimino)-acenaphthylene.

The redox activity of dpp-BIAN is provided primarily through its α-diimine backbone and secondarily by its acenaphthylene framework; it can accept up to four electrons and be conveniently isolated as the alkali metal salts, $[Na]_{1-4}$[dpp-BIAN].[25] Various dpp-BIAN salts and metal complexes have been reported.[26,27] A report of lanthanide−BIAN complexes by Cowley highlights the ability of this ligand to form neutral, mono-, and dianionic complexes by the formation of $(C_5Me_5)_xLn(BIAN)(THF)_y$ complexes of $Ln = Eu^{II}$, $x = 2$, $y = 0$; Yb^{III}, $x = 2$, $y = 0$; and Sm^{III}, $x = 1$, $y = 1$ (Scheme 1).[1]

We have found that dpp-BIAN also exhibits extensive redox activity in its complexes with the 5f elements. Herein we describe our investigations and report the synthesis and characterization of the first examples of dpp-BIAN uranium and thorium complexes, U(dpp-BIAN)$_2$ (**1**), U(dpp-BIAN)$_2$(THF) (**1-THF**), and Th(dpp-BIAN)$_2$(THF) (**2-THF**), and show that the uranium system undergoes a facile and reversible metal ion redox change in the solid state.

Scheme 1. Lanthanide−BIAN Complexes Reported by Cowley[1] Showing the Formation of Complexes with the BIAN Ligand in the Neutral, Monoanionic, and Dianionic Configurations

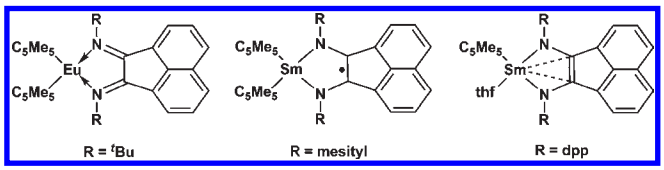

Results and Discussion

Structural Chemistry. The divalent salt of the dpp-BIAN ligand, Na_2dpp-BIAN, can be conveniently prepared in situ from the comproportionation reaction of Na_4[dpp-BIAN] (prepared from a heterogeneous reaction of dpp-BIAN with excess sodium metal) with 1 equiv of neutral dpp-BIAN.[25] Subsequent reaction with UCl_4, workup, and crystallization from hexanes/THF produced the intense purple U(dpp-BIAN)$_2$(THF) (**1-THF**) in 59% isolated yield (Scheme 2). A similar reaction with $ThBr_4(THF)_4$ and workup afforded the related purple thorium complex Th(dpp-BIAN)$_2$(THF) (**2-THF**) in 49% isolated yield. Heating crystalline solid **1-THF** to 125 °C under an inert atmosphere followed by successive evacuation and backfilling of the flask with argon gas produced the THF-free form of the complex, U(dpp-BIAN)$_2$ (**1**), in quantitative yield. X-ray-quality single crystals of **1** were similarly grown from slow evaporation of a concentrated hexane solution.

The solid-state molecular structures of **1** and **1-THF** are shown in Figure 1 and reveal that the complexes contain tetra- and pentacoordinate uranium ions, respectively, coordinated by two bidentate dpp-BIAN ligands. The molecular structure of complex **2-THF** is presented in Figure 2 and is isostructural with that of **1-THF**. The metal ion in **1** adopts a distorted tetrahedral geometry, whereas **1-THF** and **2-THF** adopt distorted square pyramidal geometries, as observed in the N−U−N angles at the uranium ions: **1**, N(1)−U(1)−N(3) = 122.8(3)°, N(2)−U(1)−N(4) = 120.8(3)°; **1-THF**, N(1)−U(1)−N(4) = 127.27(9)°, N(2)−U(1)−N(3) = 150.18(9)°. Both complexes **1** and **2-THF** crystallize with two independent molecules in their asymmetric units; the U−N bonds in **1** range from 2.244(7) to 2.283(7) Å, and the U−N bonds in **1-THF** range from 2.273(3) to 2.304(2) Å. Little structural variation was found between the α-diimine backbones of the dpp-BIAN ligands among all of the complexes. The $An-O_{THF}$ distance is 2.541(2) Å in **1-THF** and 2.556(5) and 2.574(5) Å in **2-THF**. The Th−N distances in **2-THF** are consistent with expectations defined by the U−N distances in **1**. These Th−N distances range from 2.284(6) to 2.370(6) Å; the lengthening of these distances is consistent with the ∼0.05 Å size difference between Th^{IV} and U^{IV} ions.[28]

Description of the Solid-State Electronic Structures of 1, 1-THF, and 2-THF. The electronic structures of the crystalline forms of **1**, **1-THF**, and **2-THF** were evaluated with magnetic susceptibility studies. These results, as well as those obtained in solution, are described below and summarized in Scheme 3.

(13) Berg, D. J.; Boncella, J. M.; Andersen, R. A. *Organometallics* **2002**, *21*, 4622–4631.
(14) Kuehl, C. J.; Da Re, R. E.; Scott, B. L.; Morris, D. E.; John, K. D. *Chem. Commun.* **2003**, 2336–2337.
(15) Trifonov, A. A. *Eur. J. Inorg. Chem.* **2007**, 3151–3167.
(16) Fedushkin, I. L.; Maslova, O. V.; Baranov, E. V.; Shavyrin, A. S. *Inorg. Chem.* **2009**, *48*, 2355–2357.
(17) Evans, W. J.; Davis, B. L. *Chem. Rev.* **2002**, *102*, 2119–2136.
(18) Da Re, R. E.; Jantunen, K. C.; Golden, J. T.; Kiplinger, J. L.; Morris, D. E. *J. Am. Chem. Soc.* **2005**, *127*, 682–689.
(19) Morris, D. E.; Da Re, R. E.; Jantunen, K. C.; Castro-Rodriguez, I.; Kiplinger, J. L. *Organometallics* **2004**, *23*, 5142–5153.
(20) Schelter, E. J.; Yang, P.; Scott, B. L.; Thompson, J. D.; Martin, R. L.; Hay, P. J.; Morris, D. E.; Kiplinger, J. L. *Inorg. Chem.* **2007**, *46*, 7477–7488.
(21) Graves, C. R.; Scott, B. L.; Morris, D. E.; Kiplinger, J. L. *J. Am. Chem. Soc.* **2007**, *129*, 11914–11915.
(22) Graves, C. R.; Yang, P.; Kozimor, S. A.; Vaughn, A. E.; Clark, D. L.; Conradson, S. D.; Schelter, E. J.; Scott, B. L.; Thompson, J. D.; Hay, P. J.; Morris, D. E.; Kiplinger, J. L. *J. Am. Chem. Soc.* **2008**, *130*, 5272–5285.
(23) Graves, C. R.; Scott, B. L.; Morris, D. E.; Kiplinger, J. L. *Organometallics* **2008**, *27*, 3335–3337.
(24) Graves, C. R.; Vaughn, A. E.; Schelter, E. J.; Scott, B. L.; Thompson, J. D.; Morris, D. E.; Kiplinger, J. L. *Inorg. Chem.* **2008**, *47*, 11879–11891.
(25) Fedushkin, I. L.; Skatova, A. A.; Chudakova, V. A.; Fukin, G. K. *Angew. Chem., Int. Ed.* **2003**, *42*, 3294–3298.
(26) Schumann, H.; Hummert, M.; Lukoyanov, A. N.; Chudakova, V. A.; Fedushkin, I. L. *Z. Naturforsch., B: Chem. Sci.* **2007**, *62*, 1107–1111.
(27) Schumann, H.; Hummert, M.; Lukoyanov, A. N.; Fedushkin, I. L. *Chem.—Eur. J.* **2007**, *13*, 4216–4222.
(28) Shannon, R. D. *Acta Crystallogr.* **1976**, *A32*, 751–767.

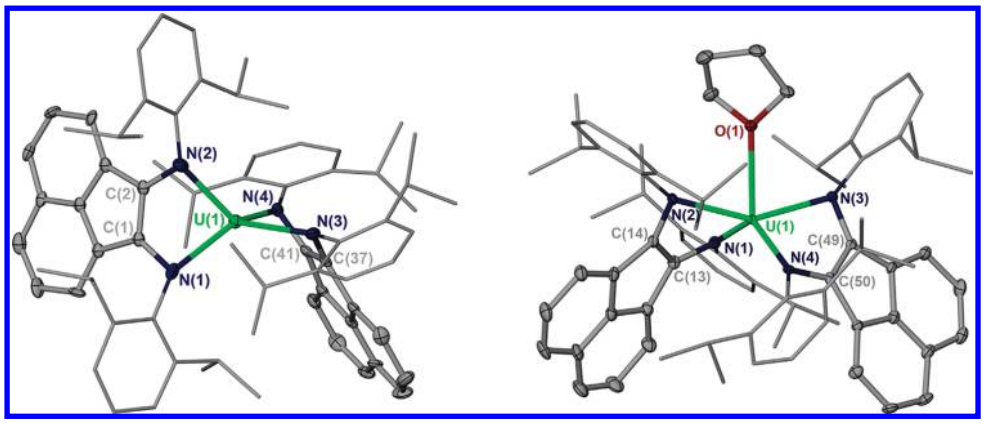

Figure 1. Molecular structures of **1** (left) and **1-THF** (right) with ellipsoids projected at the 50% probability level. Hydrogen atoms are omitted and diisopropyl-aryl group carbon atoms are depicted as spheres of arbitrary radius for clarity. Selected bond distances (Å) for **1**: U(1)−N(1), 2.252(7); U(1)−N(2), 2.260(7); U(1)−N(3), 2.283(7); U(1)−N(4), 2.247(7); N(1)−C(1), 1.415(11); N(2)−C(2), 1.395(10); N(3)−C(37), 1.378(11); N(4)−C(41), 1.407(10); C(1)−C(2), 1.410(12); C(37)−C(41), 1.412(12). For **1-THF**: U(1)−N(1), 2.273(3); U(1)−N(2), 2.291(2); U(1)−N(3), 2.280(2); U(1)−N(4), 2.304(2); N(1)−C(13), 1.405(4); N(2)−C(14), 1.396(4); N(3)−C(49), 1.393(4); N(4)−C(50), 1.404(4); C(13)−C(14), 1.407(4); C(49)−C(50), 1.400(4).

Scheme 2. Synthesis of the dpp-BIAN Uranium and Thorium Complexes **1**, **1-THF**, and **2-THF**

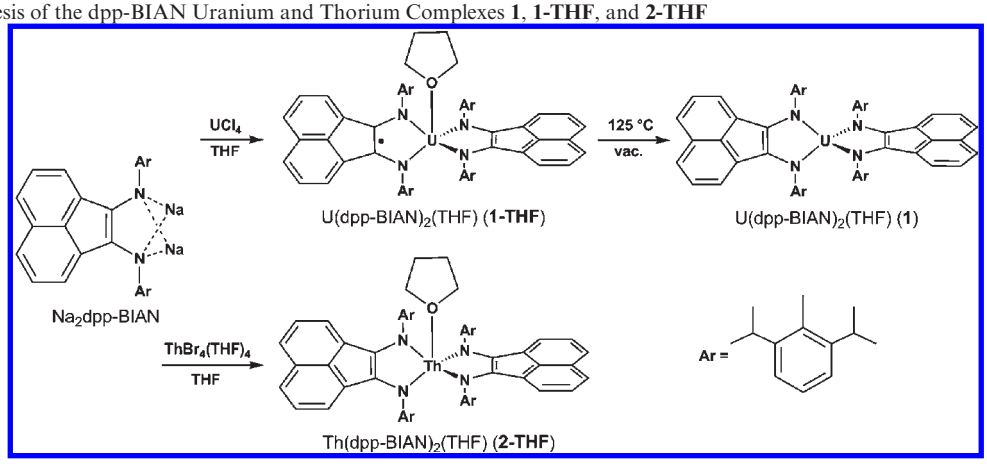

The χT product of **1** exhibits typical magnetic behavior for the U^{IV} ion (Figure 3).[20] The χT product decreases gradually from 300 to 100 K, beginning at 0.96 emu K mol^{-1} (2.77 μ_B), then descends more quickly beginning at 100 K to attain a χT product of near zero at 2 K. This temperature-dependent behavior is a reflection of the Boltzmann thermal population of the nine crystal field (CF) states for the nominal $^3H_4$ manifold in the U^{IV} ion, through reduction of the χT product by quenching of the orbital angular momentum of the $J = 4$ ground term.[29] The vanishing χT product at 2 K is consistent with a singlet, nonmagnetic ground state for this ion in its low symmetry crystal field. The temperature-dependent magnetic data for **1-THF** were found to be surprisingly different from those of **1**, as shown in Figure 3. The χT product for **1-THF** at 300 K exhibits a value of 1.71 emu K mol^{-1}. Given the value of 0.96 emu K mol^{-1} for **1**, the identical CF symmetry between **1** and **1-THF**, and the predicted maximum value of 1.6 emu K mol^{-1} for the U^{IV} ion, it is not possible that the χT product for **1-THF** is due to a single U^{IV} ion. The temperature-dependent character of χT versus T for **1-THF** (vide infra) is also dissimilar to

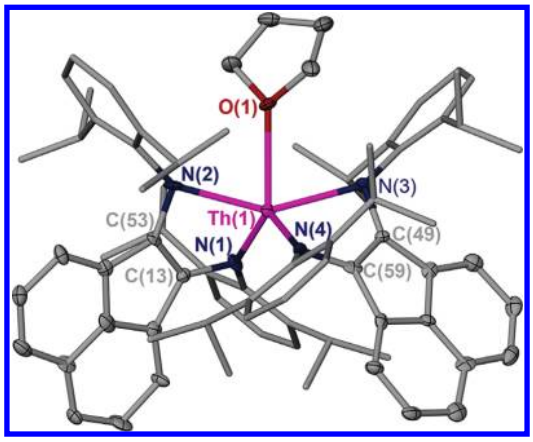

Figure 2. Molecular structure of **2-THF** with ellipsoids projected at the 50% probability level. Hydrogen atoms omitted and diisopropyl-aryl group carbon atoms depicted as spheres of arbitrary radius for clarity. Selected bond distances for **2-THF**: Th(1)−N(1), 2.348(6); Th(1)−N(2), 2.338(6); Th(1)−N(3), 2.370(6); Th(1)−N(4), 2.309(6); N(1)−C(13), 1.428(9); N(2)−C(53), 1.394(8); N(3)−C(49), 1.396(9); N(4)−C(59), 1.446(9); C(13)−C(53), 1.412(10); C(49)−C(59), 1.400(10); Th(1)−O(1), 2.556(5).

that for **1**; the χT product of **1-THF** remains fairly constant up to ~50 K, where it decreases precipitously, reaching a small finite value of 0.21 emu K mol^{-1} at 2 K.

(29) Boudreaux, E. A.; Mulay, L. N. *Theory and Applications of Molecular Paramagnetism*; John Wiley & Sons: New York, 1976.

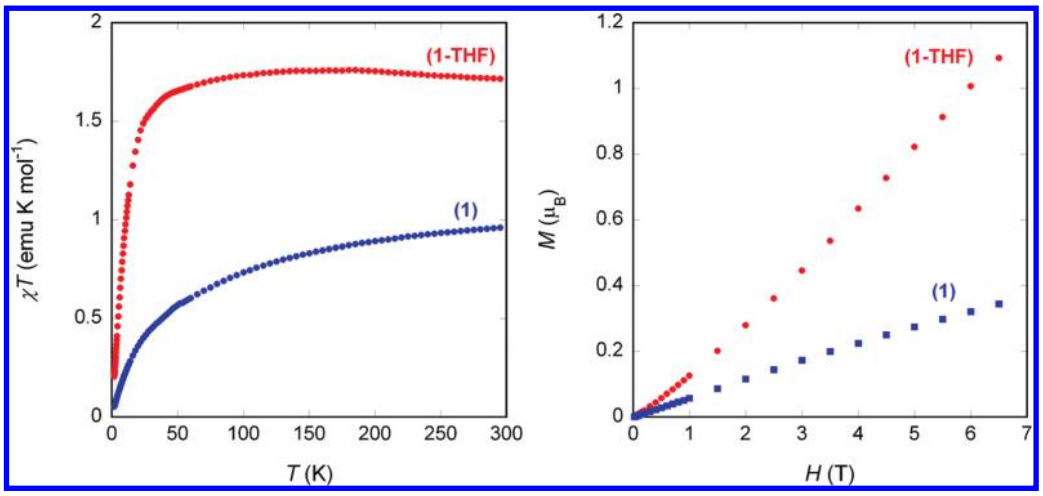

Figure 3. χT versus T data for **1** (blue trace) and **1-THF** (red trace) from 2 to 300 K (left) and field-dependent magnetization data (right) for **1** and **1-THF**.

Scheme 3. Summary of the Electronic Configurations Determined for the **1/1-THF** System under Varying Experimental Conditions

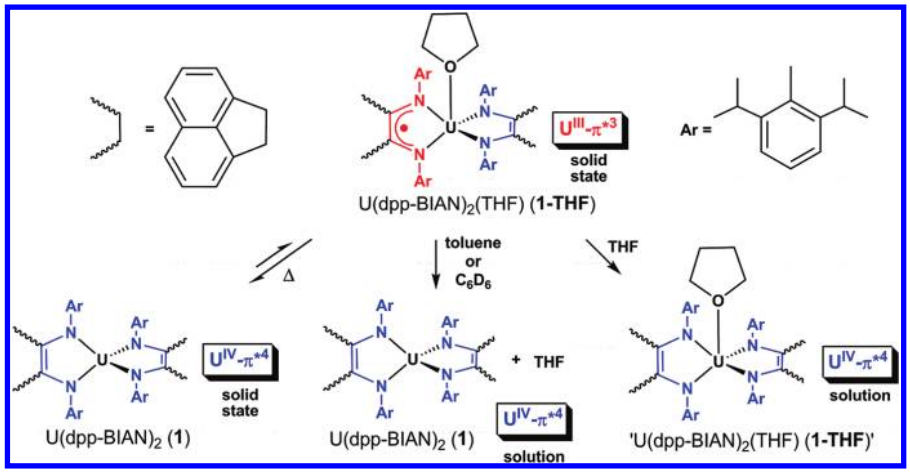

These data indicate that an electron-transfer process has occurred with the presence of THF in the uranium coordination sphere such that the ground state for **1-THF** is best represented as $U^{III}-\pi^{*3}$ (f^3 plus dpp-BIAN$^-$ ligand radical), while complex **1** exhibits a $U^{IV}-\pi^{*4}$ ground state.[30] It is commonly held that the use of magnetic data is an imprecise tool for the differentiation of U^{III} and U^{IV} complexes, due to the similar predicted χT values for the free ions using $L-S$ coupling (U^{IV}, 1.60; U^{III}, 1.64 emu K mol^{-1}). Empirically, low-symmetry crystal fields imposed by the ligands, state mixing, and partial failure of the $L-S$ coupling scheme always reduce the value of the χT products from those predicted for these ions.[31] With similar CF strengths and symmetries, phenomenological oxidation state assignment is possible.[32,33] The difference in the χT products for **1** and **1-THF** at 300 K is 0.75 emu K mol^{-1}. This value is consistent with an additional two unpaired electrons per complex in **1-THF** compared with **1**. Coupled with the essentially identical CF effects between **1** and **1-THF**, these data unequivocally preclude the assignment of both complexes as U^{IV}.

Evidence for a change in metal oxidation states between complexes **1** and **1-THF** is also found in their solid-state molecular structures. As noted above, the U−N bonds are longer in **1-THF** than in **1**, consistent with the ∼0.14 Å larger ionic radius of the U^{III} ion in **1-THF**.[28] The structural data also suggest that the position of the ligand radical hole present in **1-THF** is disordered over the two ligand sites. The $U-O_{THF}$ distances are usually uninformative with respect to the uranium oxidation state; values range from 2.42 to 2.65 Å for U^{IV} and 2.46 to 2.74 Å for U^{III}, as determined by a Cambridge Structural Database search.[34]

The temperature-dependent character of the **1-THF** susceptibility data is also consistent with assignment of U^{III} in this complex. Specifically, the five Kramer's doublet crystal field states that arise from the nominal $^4I_{9/2}$ ($5f^3$) ground term of U^{III} are significantly fewer than the nine, nondegenerate crystal field levels of U^{IV}. As such, U^{III} complexes show a sharper decrease (due to five doublets versus nine crystal field states in the absence of magnetic field) through quenching of the orbital angular

(30) $5f^3-\pi^{*3}$ and $5f^2-\pi^{*4}$ correspond to U^{III}(dpp-BIAN$^{\bullet}$)(dpp-BIAN) and U^{IV}(dpp-BIAN)$_2$ configurations, respectfully.
(31) Stewart, J. L.; Andersen, R. A. *New J. Chem.* **1995**, *19*, 587–595.
(32) Castro-Rodriguez, I.; Meyer, K. *Chem. Commun.* **2006**, 1353–1368.
(33) Schelter, E. J.; Morris, D. E.; Scott, B. L.; Thompson, J. D.; Kiplinger, J. L. *Inorg. Chem.* **2007**, *46*, 5528–5536.
(34) *Cambridge Structural Database*; Cambridge University: Cambridge, England (accessed August 2009).

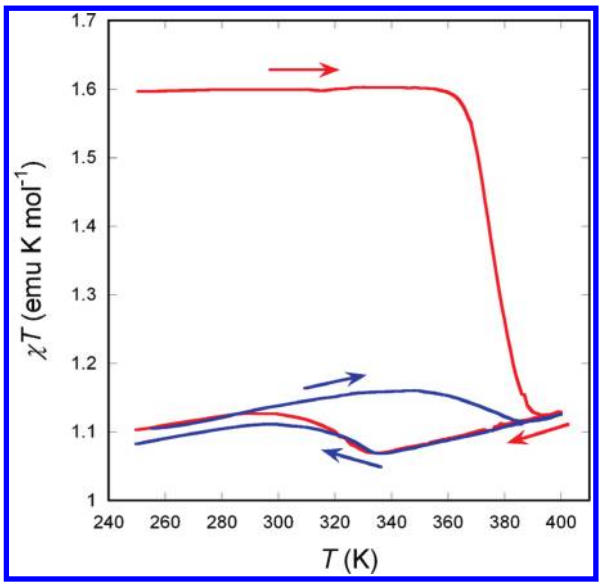

Figure 4. Elevated temperature scans of χT versus T for **1-THF** showing conversion of the complex to **1** with the associated change in oxidation state of the metal ion, and its hysteretic, partial recovery. The red trace shows the first temperature scan, while the blue trace shows the second complete scan after the complex recovers ~17% of its liberated THF. Sample aging, with concomitant loss of THF, accounts for a small reduction of the χT signal prior to onset of wholesale desolvation compared to Figure 3. Incomplete recovery is attributed to low partial pressure of THF in the sealed sample container.

momentum with decreasing temperature. This difference is present between **1** and **1-THF**; χT versus T for **1** begins to decrease gradually at ~150 K, while χT versus T for **1-THF** decreases precipitously at ~50 K. Field-dependent magnetization data collected for the complexes at 2 K are also presented in Figure 3. While neither complex achieves saturation behavior to the experimental limit of 6.5 T, the **1-THF** complex clearly shows a larger response compared to **1** over the field range probed, also supportive of a $U^{III}-\pi^{*3}$ configuration.[32] The thorium congener **2-THF** was found to be diamagnetic over the temperature range of these experiments, as expected for the ostensible $f^0-\pi^{*4}$ ($Th^{IV}-\pi^{*4}$) electronic configuration.

To further probe the origin and nature of the charge-transfer ground state in **1-THF**, the magnetic response of this complex was evaluated in an expanded temperature range. At $T \sim 360$ K (Figure 3), the χT product of **1-THF** began to decrease with the onset of THF loss from the complex (consistent with the temperature employed to synthesize and isolate **1** from **1-THF**, as noted above). That is, coordinated THF was thermally liberated in this temperature regime to effect the back-electron transfer to generate complex **1**. The drop in χT with its midpoint of ~380 K clearly illustrates this effect. As the sample was self-contained in a sealed tube (see the Experimental Section), we were also able to observe slight hysteresis with a second temperature scan as the volatilized THF was reincorporated into the structure to regenerate the charge-transfer state of **1-THF** (Figure 4), presumably with initiation of a solid−vapor equilibrium. The partial reformation of **1-THF** was estimated at ~17%, as judged by the recovery of the χT product. The assignment of the $U^{IV}-\pi^{*4}$ and $U^{III}-\pi^{*3}$ ground configurations in the crystalline forms of **1** and **1-THF**, respectively, prompted us to examine other signatures for electronic differences between the complexes.

Description of the Electronic Structures of 1 and 1-THF in Solution. The low symmetry of the complexes in the solid state creates the expectation of a localized electron hole on one of the two dpp-BIAN^{n-} ligands in **1-THF**. A common molecular orbital between the π^* NCCN backbones is not expected given the orthogonality of the N(1)−U(1)−N(2) plane to the N(3)−U(1)−N(4) plane in complex **1-THF** as is observed in the coordination angles at U(1) that describe its pseudotetrahedral coordination: N(1)−U(1)−N(4) = 127.27(9)° and N(2)−U(1)−N(3) = 150.18(9)°. The complexes were investigated in this context using electrochemistry in an effort to detect nominal ligand- and metal-based redox processes. Cyclic and square-wave voltammetry experiments were performed on complexes **1** and **1-THF**, as well as the baseline complex **2-THF** and neutral dpp-BIAN, in order to elucidate the origins of the redox waves. Measurements were performed on ~1−2 mM solutions of complexes in THF, dichloromethane, or α,α,α-trifluorotoluene (TFT) using a 0.1 M $[Bu_4N][B(3,5\text{-}(CF_3)_2\text{-}C_6H_3)_4]$ or $[Bu_4N][B(C_6F_5)_4]$ supporting electrolyte.[20,35,36] The numerical results of these studies, reported versus an internal ferrocenium/ferrocene standard, are provided as a table in the Supporting Information.

All of the complexes, as well as the free ligand, exhibit varying degrees of decomposition in the electrolyte/solvent mixtures on the time scale of the voltammetric studies, as evidenced by the appearance of new waves having lower currents than found for the starting analytes. Despite the instability, we were able to generalize the appearance of reversible or quasi-reversible redox processes for the complexes. For the neutral dpp-BIAN ligand, in either THF or TFT, a reversible one-electron reduction wave is observed at −2.12 V, which is assigned to the reduction of the α-diimine backbone of the dpp-BIAN ligand to generate dpp-BIAN$^-$ (π^{*1}). A second, quasi-reversible reduction is also observed for the ligand at −2.56 V (π^{*2}). On complexation to either uranium or thorium ions, two reversible or quasi-reversible waves are evident for the complexed dpp-BIAN^{2-} ligands. Assignment of these waves to ligand-based processes in all cases can be made from comparison of the data for the d^0f^0 thorium complex **2-THF**, which is not expected to exhibit metal-based redox processes. The first primary redox process of the complexes, a ligand-based oxidation, occurs between −0.37 and −0.48 V, depending on solvent and electrolyte identity. The reversibility of this ligand oxidation is also dependent on experimental conditions. The second primary redox process occurs within a wider window between complexes, showing a range of −2.31 to −2.55 V and a greater sensitivity to experimental conditions. The presence of THF, either in the starting complex or as the solvent, has little effect on the observed half-wave potentials.

The lack of readily identifiable metal-based redox processes for the uranium complexes **1** and **1-THF** under any experimental conditions means that the voltammetric data provide no additional insight into the metal

(35) Barriere, F.; Geiger, W. E. *J. Am. Chem. Soc.* **2006**, *128*, 3980–3989.
(36) Ohrenberg, C.; Geiger, W. E. *Inorg. Chem.* **2000**, *39*, 2948–2950.

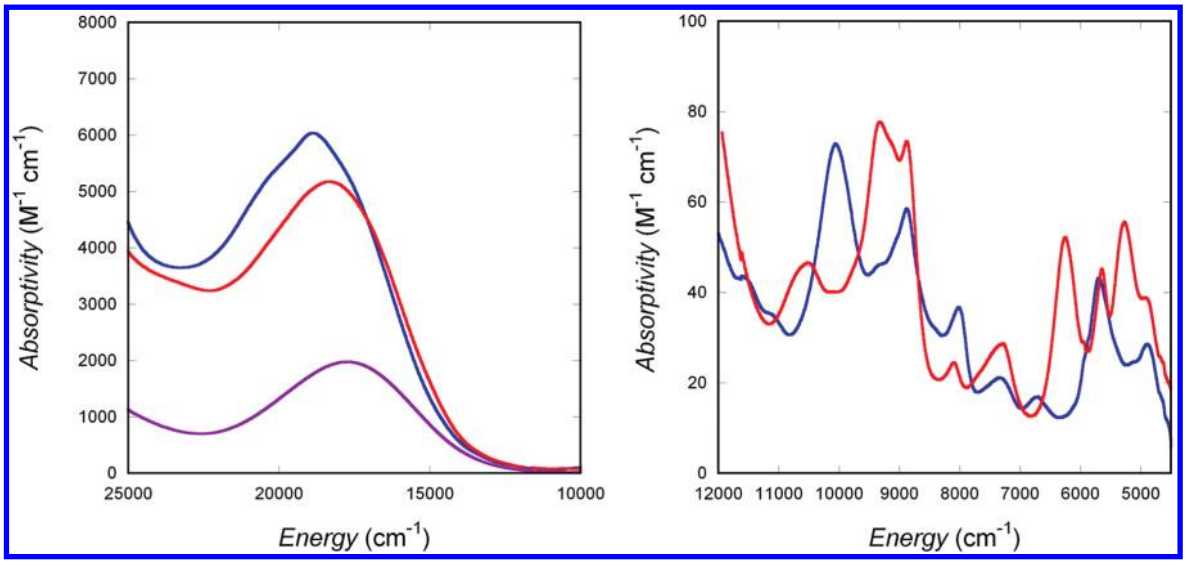

Figure 5. UV−visible, near-IR electronic absorption data for **1** (blue trace), **1-THF** (red trace), and **2-THF** (purple trace) in the $\pi-\pi^*$ (left) and f−f (right) transition energy regions.

oxidation state or the possibility for an oxidation-state transition upon solvent coordination, as seen for the solid-state complexes. This apparent lack of metal-based redox processes in **1** and **1-THF** is noteworthy but not without precedent. In our previous studies on multimetallic complexes derived from the uranium(IV) ketimide complex $(C_5Me_5)_2U[-N{=}C(Bn)(tpy)]_2$ (where Bn = CH_2-C_6H_5, tpy = terpyridyl), U^{IV}-based redox chemistry is seen for the monometallic precursor, but when additional $(C_5Me_4Et)_2U^{III}$ moieties are ligated by the two tpy functional groups, evidence for redox chemistry associated with the bridging U^{IV} ion is no longer observed.[37,38]

Since the electrochemistry of the complexes revealed no significant differences between **1** and **1-THF**, in the presence or absence of THF, further investigations of the behavior of the complexes in solution were pursued. Solution ^{1}H NMR provided several important insights. The ^{1}H NMR resonances for **1** and **1-THF**, collected in benzene-d_6 and tetrahydrofuran-d_8, respectively, display the typical paramagnetically broadened and shifted signals observed for trivalent and tetravalent uranium coordination complexes. The range of signals for the two complexes is remarkably similar: **1** displays resonances from δ +40 to −45 ppm, while the resonances for **1-THF** range from δ +37 to −43 ppm. Both complexes possess C_2 symmetry in solution. The solution magnetic moment of **1-THF** was determined in tetrahydrofuran-d_8 using the Evans method to have a χT product of 0.97 emu K mol^{-1} (2.79 μ_B).[39] (The solution magnetic moment of **1** could not be measured reliably by this method because of its low solubility in both benzene-d_6 and toluene-d_8.) Comparison with the temperature-dependent magnetic data for crystalline **1-THF** (1.71 emu K mol^{-1}) and **1** (0.96 emu K mol^{-1}) at ambient temperature reveals that **1-THF** clearly exhibits a $U^{IV}-\pi^{*4}$ ground-state electronic configuration in solution. The identity of **1-THF** as a uranium(IV) complex in solution is consistent with the results of the electrochemical experiments for the ligand-based processes, which showed little difference between measurements collected across the various solvents and electrolyte combinations. These results support an expected subtle difference between redox states for **1-THF**, which exists in a $U^{III}-\pi^{*3}$ configuration in the solid state but a $U^{IV}-\pi^{*4}$ configuration in solution (Scheme 3).

Solution UV−vis−NIR measurements for complexes **1**, **1-THF**, and **2-THF** collected in toluene and THF are presented in Figure 5. The spectroscopic features for these species are differentiated into high- and low-energy regimes between 12 000 and 25 000 and 4500−12 000 cm^{-1}, respectively. Above 12 000 cm^{-1}, all of the complexes exhibit a broad, intense feature. Complex **2-THF** exhibits this transition centered at 17 800 cm^{-1}. The absence of valence d or f electrons in the thorium complex **2-THF**, as well as its broad, intense character, affords assignment of this transition as ligand-based $\pi-\pi^*$ (or $\pi^*-\pi^*$), an assignment that can be extended to the analogous transitions in **1** and **1-THF**. Complex **1** shows this transition at 18 900 cm^{-1} with a higher-energy shoulder at ∼20 400 cm^{-1}, while this primary transition in complex **1-THF** is shifted to 18 300 cm^{-1}, and the shoulder is no longer evident. A clean isosbestic point appears at 17 100 cm^{-1} on titration of the solutions of **1** with THF, showing the conversion of **1** to **1-THF** (see the Supporting Information), although nonlinearity in the concentration dependence of the data precludes the derivation of an equilibrium constant for the formation of the solvent-coordinated complex. The relatively small shift of ∼550 cm^{-1} of the primary band between complexes **1** and **1-THF** is consistent with a reorganization of the coordination sphere geometry upon the coordination of THF[40−44] and agrees with the orbital energy

(37) Schelter, E. J.; Veauthier, J. M.; Thompson, J. D.; Scott, B. L.; John, K. D.; Morris, D. E.; Kiplinger, J. L. *J. Am. Chem. Soc.* **2006**, *128*, 2198–2199.
(38) Schelter, E. J.; Wu, R.; Scott, B. L.; Thompson, J. D.; Morris, D. E.; Kiplinger, J. L. *Angew. Chem., Int. Ed.* **2008**, *47*, 2993–2996.
(39) Naklicki, M. L.; White, C. A.; Plante, L. L.; Evans, C. E. B.; Crutchley, R. J. *Inorg. Chem.* **1998**, *37*, 1880–1885.
(40) Malek, C. K.; Krupa, J. C.; Genet, M. *Spectrochim. Acta, Part A* **1986**, *42A*, 907–912.
(41) Van Der Sluys, W. G.; Berg, J. M.; Barnhardt, D.; Sauer, N. N. *Inorg. Chim. Acta* **1993**, *204*, 251–256.
(42) Fielden, J.; Long, D.-L.; Cronin, L. *Chem. Commun.* **2004**, 2156–2157.

predictions from geometry-optimized DFT calculations (vide infra).

Compared to the higher-energy bands for **1** and **1-THF**, the transitions appearing between 4500 and 12 000 cm^{-1} are significantly less intense and narrower, consistent with their assignment as intraconfigurational f−f bands. Although there is some variation between the spectra of **1** and **1-THF** in this region, specifically the appearance of new bands at 9330, 6270, and 5270 cm^{-1}, the energy range and intensity of the f−f bands between these complexes also indicate minimal alteration, inconsistent with expectations for a change in metal oxidation state with THF coordination. Lower-energy ligand-field transitions are not observed for **2-THF**, consistent with the d^0f^0 configuration of the Th^{IV} ion. The absence of an interconfigurational $f^3 \rightarrow f^2d^1$ transition in the spectrum of **1-THF** also provides supporting evidence for its assignment as a U^{IV} complex in solution. Overall, changes in the absorption spectrum of **1** with the addition of THF are also inconsistent with a change in the oxidation state of the complex in solution; rather, the changes in the presence of THF are due to a relatively minor modification of the local geometry of the metal ion by coordination of the solvent.

Summary of the Electronic Structures of 1 and 1-THF in Solution and the Solid State. A representation of the electronic configurations for the **1**/**1-THF** system under the experimental conditions is presented in Scheme 3. Complex **1-THF** exists as a $U^{III}-\pi^{*3}$ complex in the solid state and can be converted to the $U^{IV}-\pi^{*4}$ complex **1** reversibly with thermal cycling. However, in both the presence and absence of THF, the electronic configurations of the complexes in solution are consistent with a $U^{IV}-\pi^{*4}$ assignment. Recent reports have shown that "charge separation" complexes result from one-electron reduction chemistry starting from a U^{III} complex, which becomes oxidized with the coordination of small molecules such as CO_2,[45] diazomethane,[46] benzophenone,[47] or pyrazine.[48] Of these, the bimetallic pyrazine reduction is the most relevant given its reported reversibility; however, the uniqueness of the **1/1-THF** system is that the donor molecule is not involved in the electron transfer.

A striking aspect of the **1/1-THF** system is the solution configuration of **1-THF** as $U^{IV}-\pi^{*4}$ (Scheme 3). A reversible, THF-mediated redox reaction has been reported for $(C_5Me_5)Eu(DADC_6F_5)$ ($DADC_6F_5 = C_6F_5NC(Me)C(Me)NC_6F_5$).[49] The solid-state electronic configuration of this complex is $Eu^{III}-\pi^{*1}$, whereas dissolution results in the generation of Eu^{II} with a concomitant loss of the neutral $DADC_6F_5$ ligand, similar to the results observed for **1-THF**, as shown in Scheme 3. Recent results have also demonstrated the ability of a Yb−(dpp-BIAN) complex to show temperature-dependent valence changes in solution.[16] In addition, a self-contained two-electron oxidation state change has been reported for a Ge^{II} complex of the redox-active tetraphenylporphyrin^{2-} (TPP) ligand, which converts to the Ge^{IV} upon the coordination of pyridine.[50] The oxidation state change in this case results from the conversion of the aromatic $Ge^{II}(TPP)$ complex to the antiaromatic $Ge^{IV}(TPP)(py)_2$ on the coordination of pyridine. The accessibility of the two-electron charge-transfer state in $Ge^{IV}(TPP)(py)_2$ clearly regulates this conversion. Together with the **1**/**1-THF** system, this body of work indicates significant electronic flexibility of the f-element redox couples in complexes supported by redox-active ligand sets. More specifically, the redox change at the uranium metal center upon conversion of **1-THF** to **1** with release of the THF ligand is likely due to stabilization and relaxation of the coordination sphere, specifically the redox-active π^* orbitals of the α-diimine backbone of the dpp-BIAN^{n-} ligands.

DFT and CASSCF Calculations of 1 and 1-THF. The electronic structures of **1** and **1-THF** were examined using density functional theory calculations to gain further information about the ground states of these complexes. No simplified model compounds were used in the calculations. Overall, the optimized geometries were in good agreement with the X-ray diffraction results, with the experimentally observed lengthening of the average U−N bond distances for **1-THF** compared to **1** being reproduced in the calculated structures within 0.01 Å. The distinction between the ground states for **1** and **1-THF** was expected to be subtle, stemming from different degrees of electron localization between the metal center and one or both dpp-BIAN ligands. Using hybrid density functional theory (B3LYP), which corrects the overdelocalization introduced by the LDA and GGA functionals, the calculated gas-phase electronic structures of **1** and **1-THF** *both* yield a U^{IV} ground state with a net spin of 2.2, which is contrary to the experimental magnetic data for **1-THF** in the solid state. This is not surprising given the difficulties with performing electronic structure calculations on electronic broken-symmetry systems. The binding energy of the THF ligand in complex **1** was calculated to be −2.3 kcal/mol, indicating that it is weakly bound to the uranium metal center and can undergo rapid exchange at room temperature. The presence of free THF is evident experimentally in the ^1H NMR spectrum of **1-THF** collected in benzene-d_6 at 297 K.

Significant differences between **1** and **1-THF** do arise in the electronic structure calculations, which may support the observed reversible charge-transfer state. An energy level diagram with the metal orbital components is shown in Figure 6. The unpaired spin density is located in the f_σ and f_ϕ uranium orbitals, which are the two orbitals that minimize the effect of the ligand field. HOMO and HOMO−1 are orbitals based on the dpp-BIAN ligand with more than 50% of the charge density in the α-diimine

(43) Livoreil, A.; Sauvage, J.-P.; Armaroli, N.; Balzani, V.; Flamigni, L.; Ventura, B. *J. Am. Chem. Soc.* **1997**, *119*, 12114–12124.
(44) Sato, Y.; Ohkoshi, S.; Arai, K.; Tozawa, M.; Hashimoto, K. *J. Am. Chem. Soc.* **2003**, *125*, 14590–14595.
(45) Castro-Rodriguez, I.; Nakai, H.; Zakharov, L. N.; Rheingold, A. L.; Meyer, K. *Science* **2004**, *305*, 1757–1760.
(46) Lam, O. P.; Feng, P. L.; Heinemann, F. W.; O'Connor, J. M.; Meyer, K. *J. Am. Chem. Soc.* **2008**, *130*, 2806–2816.
(47) Lam, O. P.; Anthon, C.; Heinemann, F. W.; O'Connor, J. M.; Meyer, K. *J. Am. Chem. Soc.* **2008**, *130*, 6567–6576.
(48) Mehdoui, T.; Berthet, J.-C.; Thuery, P.; Ephritikhine, M. *Eur. J. Inorg. Chem.* **2004**, 1996–2000.
(49) Moore, J. A.; Cowley, A. H.; Gordon, J. C. *Organometallics* **2006**, *25*, 5207–5209.
(50) Cissell, J. A.; Vaid, T. P.; Yap, G. P. A. *J. Am. Chem. Soc.* **2007**, *129*, 7841–7847.

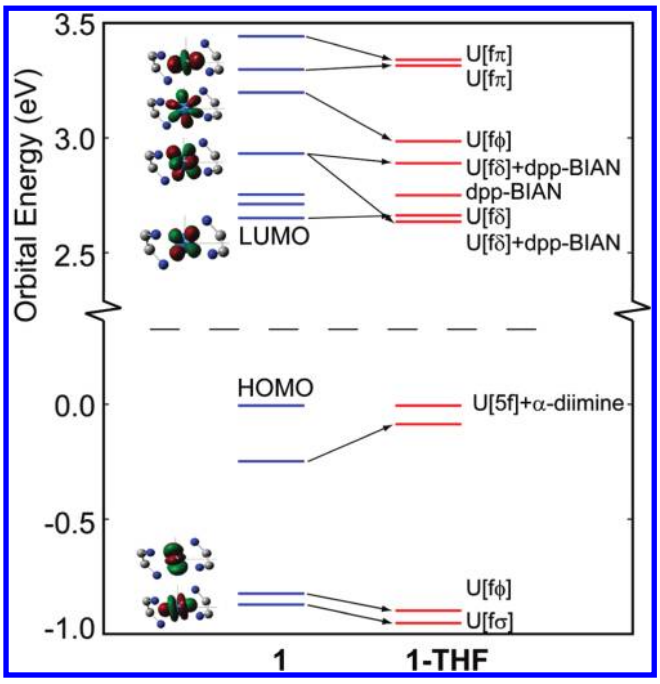

Figure 6. Orbital level diagram obtained from hybrid DFT for complexes **1** and **1-THF**. The left column presents a picture of the orbital metal component, and the orbital character is shown on the right column.[51] Upon coordination of a THF solvent molecule to complex **1**, the α-diimine-based orbital is destabilized while the unoccupied metal 5f orbitals are stabilized, facilitating the observed charge-transfer for **1-THF**. For clarity, only the α atoms are shown, although no simplified model complexes were used in the electronic structure calculations.

fragments and 10−20% mixed uranium 5f character.[51] The lowest unoccupied orbitals consist of the five uranium 5f orbitals plus two π^* orbitals from the dpp-BIAN ligands (LUMO+1 and LUMO+2 in complex **1**). Upon the coordination of THF, the metal orbitals in **1-THF** are stabilized relative to what they are in complex **1**. In particular, the LUMO+3 orbital, which is mostly a metal $5f_\delta$ orbital in complex **1**, is stabilized and mixes with the ligand orbital LUMO+1 to yield the **1-THF** orbitals LUMO and LUMO+3, leading to a lowering in energy of up to 0.3 eV. All of the other metal 5f orbitals also are stabilized upon the coordination of THF, but to a smaller extent.

Simultaneously, upon the coordination of THF, the HOMO−1 orbital in **1-THF** is raised in energy relative to what it is in **1**. Linear response theory was used to calculate the lowest triplet−triplet excitations to compare the energy of the charge-separated states in the two molecules. For complex **1**, the lowest charge-transfer state is a $U^{III}-\pi^{*3}$ configuration due to a HOMO → LUMO charge transfer. In complex **1-THF**, three charge-transfer states were found to be lower in energy than that in complex **1**, by 0.12, 0.11, and 0.02 eV.[51] Although convergence to a ground-state $U^{III}-\pi^{*3}$ configuration was not attained for **1-THF**, the calculations suggest that a charge transfer from the ligand to the metal is more feasible for **1-THF** compared to complex **1**.

To further scrutinize the results of the DFT calculations for **1-THF** and to evaluate for significant admixture of multiple configurations in the ground state of the complex, we performed complete active space self-consistent field (CASSCF) calculations on the structure optimized by DFT. The active space included six electrons in the top four occupied and three lowest virtual orbitals. The isopropyl groups were removed, and correlation corrections were not included, as the calculations were performed at the limit of our computational capacity. Overall, the ground state obtained from CASSCF for **1-THF** was identical to the one obtained from DFT-B3LYP. A full output of the CASSCF calculations is included as Supporting Information. The two lowest excited states predicted by CASSCF were found to be 2.84 and 3.74 eV higher in energy than the ground state, respectively; however, these energies are likely overestimated by the missing correlation energy. The electronic state of the first excited state was found to have significant contributions from several determinants; therefore, it is difficult to give a single particle picture. The most prominent determinants involve charge-transfer excitations from the diimine ligand into the uranium 5f orbitals and into the acenaphthylene moiety with the spin state of the f electrons corresponding to a combination of quartet multiplicity (determinant 106) and doublet states (determinant 15). As with the DFT-B3LYP, the excited state structure points to a complex charge-transfer picture for **1-THF**, lying energetically proximate to, but unmixed with, the $5f^2$ configuration.

Conclusions

We have presented a uranium complex of the redox-active ligand dpp-BIAN that undergoes a facile and reversible redox change upon desolvation. The complexes **1-THF** and **2-THF** can be easily prepared and isolated in good yields; heating/evacuation of samples of **1-THF** produced the unsolvated complex **1** in quantitative yields. Magnetic and structural data reveal that complex **1** exhibits a $U^{IV}-\pi^{*4}$ ground-state electronic configuration, while **1-THF** is $U^{III}-\pi^{*3}$. Temperature cycling of **1-THF** affords the liberation and partial recoordination of THF to effect reversible redox changes in the complex in the solid state. This represents a rare example of a well-defined reversible intramolecular electron transfer for an f-element complex and further exemplifies the unique electronic structure aspects of uranium complexes.

We postulate that the presence of THF in the coordination sphere of **1-THF** causes steric pressure on the α-diimine backbone of the dpp-BIAN ligands, resulting in a destabilization that finds an energetic minimum on electron transfer and concomitant elongation of the $U^{III}-N$ bonds in **1-THF**. This is supported by the DFT calculations and spectroscopic data, which suggest that a charge transfer from the ligand to the metal is more feasible for **1-THF** compared to complex **1**. Although preliminary reactivity studies of **1** and **1-THF** with small molecules have shown complex decomposition in all cases, the physicochemical studies presented here represent an interesting look at the properties of 5f-element complexes of redox-active ligands.

Experimental Section

General Synthetic Considerations. Unless otherwise noted, reactions and manipulations were performed at 25 °C in a recirculating Vacuum Atmospheres NEXUS inert atmosphere

(51) See Tables S4−S7 in the Supporting Information for a detailed output of the exact orbital populations for complexes **1** and **THF-1**.

(N_2) drybox equipped with a 40CFM Dual Purifier NI-Train, or using standard Schlenk line techniques. Glassware was dried overnight at 150 °C before use. All NMR spectra were obtained in either tetrahydrofuran-d_8 or benzene-d_6 using a Bruker Avance 300 MHz spectrometer. Chemical shifts for ^{1}H NMR spectra were referenced to solvent impurities. Elemental analyses were performed at the University of California, Berkeley Microanalytical Facility, on a Perkin-Elmer Series II 2400 CHNS analyzer.

Unless otherwise noted, reagents were purchased from commercial suppliers and used without further purification. Celite (Aldrich), alumina (Brockman I, Aldrich), and 4 Å molecular sieves (Aldrich) were dried under a dynamic vacuum at 250 °C for 48 h prior to use. Hexane (anhydrous, Aldrich), tetrahydrofuran (anhydrous, Aldrich), toluene (anhydrous, Aldrich), and bis(trimethylsilyl)ether (Aldrich) were dried over KH for 24 h, passed through a column of activated alumina under nitrogen, and stored over activated 4 Å molecular sieves prior to use. α,α,α-Trifluorotoluene (anhydrous, Aldrich) was passed through a column of activated alumina under nitrogen and stored over activated 4 Å molecular sieves prior to use. Benzene-d_6 (Aldrich) and tetrahydrofuran-d_8 (Cambridge Isotope Laboratories) were purified by storage over activated 4 Å molecular sieves under N_2 prior to use. UCl_4,[52] $ThBr_4(THF)_4$,[53] $[Bu_4N][B(C_6F_5)_4]$,[54−57] $[Bu_4N][B(3,5\text{-}(CF_3)_2\text{-}C_6H_3)_4]$,[35] and 1,2-bis(2,6-diisopropylphenylimino)acenaphthylene (dpp-BIAN)[58] were prepared according to literature procedures.

Caution! *Depleted uranium (primarily isotope ^{238}U) and natural thorium (^{232}Th) are weak α-emitters with half-lives of 4.47×10^9 years and 1.41×10^{10} years, respectively; manipulations and reactions should be carried out in monitored fume hoods or in an inert atmosphere drybox in a radiation laboratory equipped with α- and β-counting equipment.*

Note: Complexes **1-THF**, **1**, and **2-THF** were observed to be unstable, even on storage in the solid state at −30 °C, noted by the appearance of two sets of ^{1}H resonances (doublets) at $\delta \sim 1.19$ and 1.09 ppm (depending on the solvent). These peaks are attributed to a form of uncomplexed dpp-BIAN. All characterization measurements were performed on fresh samples whose purity was checked by ^{1}H NMR spectroscopy.

Synthesis of U(dpp-BIAN)$_2$(THF) (1-THF). A 20 mL scintillation vial was charged with dpp-BIAN (0.31 g, 0.62 mmol), sodium metal (0.34 g, 14.57 mmol, 23.5 equiv), and tetrahydrofuran (10 mL). The resulting clear, orange solution was stirred for 16 h to produce a dark brown suspension. The brown suspension was decanted from the remaining sodium metal and added to a clear, orange tetrahydrofuran solution of dpp-BIAN (0.31 g, 0.62 mmol, 1.0 equiv) in a 20 mL scintillation vial, which initiated an immediate change to a dark orange/green dichroic solution. This mixture was stirred for 30 min, and solid UCl_4 (0.23 g, 0.62 mmol, 0.5 equiv) was added, resulting in an immediate color change to dark purple. The dark purple solution was stirred for 2 h and filtered through a Celite-packed coarse porosity frit and the volatiles removed from the filtrate under reduced pressure. The dark purple, wet residue was extracted with hexanes (2 × 20 mL) and filtered through a Celite-packed coarse porosity frit. The combined dark purple solutions were chilled overnight at −30 °C to deposit crystalline **1-THF**. The supernatant was decanted off and the crystals washed with bis(trimethylsilyl)ether (4 × 10 mL) and dried under reduced pressure for 10 min. Further chilling the mother liquor at −30 °C produced two additional batches of purple crystals (combined yield: 0.48 g, 0.36 mmol, 59%). ^{1}H NMR (tetrahydrofuran-d_8, 298 K): δ 36.56 (br s, 2H, −CH(CH$_3$)$_2$), 26.32 (br s, 2H, −CH-(CH$_3$)$_2$), 23.92 (d, J = 7.8 Hz, 2H, Ar−H), 21.28 (s, 6H, −CH-(CH_3)$_2$), 19.07 (d, J=7.5 Hz, 2H, Ar−H), 18.17 (d, J=9.0 Hz, 2H, Ar−H), 15.64 (t, J = 7.5 Hz, 2H, Ar−H), 13.87 (s, 6H, −CH-(CH_3)$_2$), 7.34 (s, 6H, −CH(CH_3)$_2$), 7.22 (s, 2H, Ar−H), 6.72 (d, J = 6.9 Hz, 2H, Ar−H), −0.58 (s, 6H, −CH(CH_3)$_2$), −0.63 (s, 6H, −CH(CH_3)$_2$), −1.48 (d, J = 7.8 Hz, 2H, Ar−H), −1.87 (t, J = 7.2 Hz, 2H, Ar−H), −2.50 (d, J = 6.9 Hz, 2H, Ar−H), −14.45 (s, 6H, −CH(CH_3)$_2$), −18.36 (br s, 2H, −CH(CH$_3$)$_2$), −20.01 (d, J = 3.0 Hz, 2H, Ar−H), −42.38 (s, 6H, −CH(CH_3)$_2$), −42.48 (s, 6H, −CH(CH_3)$_2$); additional resonances for **1-THF** were not observed. ^{1}H NMR of **1-THF** (297 K) recorded in benzene-d_6 showed the presence of free THF at δ 3.90 and 1.88. Anal. Calcd for $C_{76}H_{88}N_4OU$ (1311.57 g/mol): C, 69.60; H, 6.76; N, 4.27. Found: C, 69.49; H, 6.79; N, 4.45.

Synthesis of U(dpp-BIAN)$_2$ (1). A 50 mL thick-walled Schlenk tube equipped with a Teflon valve was charged with **1-THF** (0.10 g, 0.078 mmol). The vessel was heated to 125 °C under Ar for 1 h, then evacuated, and backfilled, resulting in quantitative conversion of **1-THF** to **1**. X-ray-quality single crystals of **1** were grown from slow evaporation of a concentrated hexane solution. ^{1}H NMR (benzene-d_6, 296 K): δ 40.28 (m, 2H, −CH-(CH$_3$)$_2$), 27.49 (m, 2H, −CH(CH$_3$)$_2$), 16.08 (d, J = 7.5 Hz, 2H, Ar−H), 12.22 (d, J = 5.7 Hz, 2H, Ar−H), 12.09 (d, J = 4.5 Hz, 6H, −CH(CH_3)$_2$), 9.66 (d, J = 7.2 Hz, 2H, Ar−H), 9.14 (two overlapping doublets, 12H, −CH(CH_3)$_2$), 8.85 (overlapping multiplets, 6H, −CH(CH$_3$)$_2$ and Ar−H), 7.30 (d, J = 8.1 Hz, 2H, Ar−H), 7.04 (t, J = 7.5 Hz, 2H, Ar−H), 5.29 (t, J = 7.5 Hz, 2H, Ar−H), 5.19 (d, J = 6.6 Hz, 2H, Ar−H), 4.94 (d, J = 6.9 Hz, 2H, Ar−H), 4.40 (t, J = 7.2 Hz, 2H, Ar−H), 3.10 (d, J = 7.2 Hz, 2H, Ar−H), 1.09 (d, J=6.9 Hz, 2H, Ar−H), 0.61 (d, J=5.1 Hz, 6H, −CH(CH_3)$_2$), −0.68 (s, 6H, −CH(CH_3)$_2$), −8.07 (s, 6H, −CH(CH_3)$_2$), −22.85 (s, 6H, −CH(CH_3)$_2$), −32.38 (s, 6H, −CH(CH_3)$_2$), −45.09 (br s, 2H, −CH(CH$_3$)$_2$). Anal. Calcd for $C_{72}H_{80}N_4U$ (1239.46 g/mol): C, 69.77; H, 6.51; N, 4.52. Found: C, 69.47; H, 6.74; N, 4.85.

Synthesis of Th(dpp-BIAN)$_2$(THF) (2-THF). The synthesis of **2-THF** from $ThBr_4(THF)_4$ (0.43 g, 0.51 mmol), dpp-BIAN (0.51 g, 1.02 mmol, 2 equiv), and sodium metal (0.32 g, 13.70 mmol, 27 equiv) is identical to **1-THF**. Yield of purple crystalline **2-THF**: 0.32 g, 0.25 mmol, 49%. ^{1}H NMR (tetrahydrofuran-d_8, 298 K): δ 7.24 (m, 4H, Ar−H), 7.04 (m, 4H, Ar−H), 6.88 (t, J = 7.8 Hz, 2H, Ar−H), 6.81 (t, J=7.8 Hz, 2H, Ar−H), 6.40 (d, J = 6.9 Hz, 2H, Ar−H), 6.30 (d, J = 6.6 Hz, 2H, Ar−H), 3.63 (s, 8H, β-H-THF), 3.48 (m, 6H, −CH(CH$_3$)$_2$), 3.23 (m, 2H, −CH-(CH$_3$)$_2$), 1.29 (s, 8H, α-H-THF), (br d, J = 7.2 Hz, 12H, −CH-(CH_3)$_2$), 1.13 (d, J = 6.6 Hz, 6H, −CH(CH_3)$_2$), 0.96 (two overlapping doublets, 12H, −CH(CH_3)$_2$), (br, d, J = 6.3 Hz, 12H, −CH(CH_3)$_2$), 0.19 (d, J=6.0 Hz, 6H, −CH(CH_3)$_2$); additional aryl resonances overlap with the protio impurity solvent peak. Anal. Calcd for $C_{76}H_{88}N_4OTh$ (1305.58 g/mol): C, 69.92; H, 6.79; N, 4.29. Found: C, 69.69; H, 7.08; N, 4.28.

Electronic Absorption Spectroscopy. Electronic absorption spectral data were obtained for THF and toluene solutions of complexes **1**, **1-THF**, and **2-THF** over the wavelength range 280−2500 nm on a Perkin-Elmer Model Lambda 950 UV−visible−NIR spectrophotometer. All data were collected in 1 mm path length cuvettes loaded in the Vacuum Atmospheres drybox system described above. Samples were run at multiple concentrations to optimize absorbance in the UV−visible and near-infrared, respectively. Spectral resolution was typically 2 nm in the visible region and 4−6 nm in the near-infrared.

(52) Kiplinger, J. L.; Morris, D. E.; Scott, B. L.; Burns, C. J. *Organometallics* **2002**, *21*, 5978–5982.
(53) Clark, D. L.; Frankcom, T. M.; Miller, M. M.; Watkin, J. G. *Inorg. Chem.* **1992**, *31*, 1628–1633.
(54) Barriere, F.; LeSuer, R. J.; Geiger, W. E. *Trends Mol. Electrochem.* **2004**, 413–444.
(55) LeSuer, R. J.; Buttolph, C.; Geiger, W. E. *Anal. Chem.* **2004**, *76*, 6395–6401.
(56) LeSuer, R. J.; Geiger, W. E. *Angew. Chem., Int. Ed.* **2000**, *39*, 248–250.
(57) Nafady, A.; Costa, P. J.; Calhorda, M. J.; Geiger, W. E. *J. Am. Chem. Soc.* **2006**, *128*, 16587–16599.
(58) Paulovicova, A.; El-Ayaan, U.; Shibayama, K.; Morita, T.; Fukuda, Y. *Eur. J. Inorg. Chem.* **2001**, 2641–2646.

Computational Methodology. The B3LYP hybrid density functional[59] was employed to study the electronic structure of the model complexes. Both complexes, **1** and **1-THF**, were optimized with no symmetry constraint using an unrestricted open shell formalism. The Stuttgart RSC 1997 ECP[60−62] was employed for the uranium center, which incorporates scalar relativistic effects and replaces 60 core electrons. The valence electrons are represented as [8s/7p/6d/4f]; 6-31G* basis sets were used for carbon, hydrogen, and nitrogen. For the CASSCF calculations, the converged molecular orbitals from B3LYP hybrid density functional theory were used when defining the active space, and the geometry of the molecule was kept fixed at the DFT optimized one. The same basis set and effective core potentials were used as described above. All calculations were carried out using the *Gaussian 03* suite of codes.[63]

Electrochemistry. Cyclic wave voltammetric data were obtained in the Vacuum Atmospheres drybox system described above. All data were collected using a Perkin-Elmer Princeton Applied Research Corporation (PARC) Model 263 potentiostat under computer control with PARC Model 270 software. All sample solutions were ∼2−3 mM in complex with a 0.1 M $[Bu_4N][B(C_6F_5)_4]$ or $[Bu_4N][B(3,5\text{-}(CF_3)_2\text{-}C_6H_3)_4]$ supporting electrolyte in THF or α,α,α-trifluorotoluene (TFT). All data were collected with the positive-feedback IR compensation feature of the software/potentiostat activated to ensure minimal contribution to the voltammetric waves from uncompensated solution resistance (typically ∼1 kΩ under the conditions employed). Solutions were contained in PARC Model K0264 microcells consisting of a ∼3-mm-diameter Pt disk working electrode, a Pt wire counter-electrode, and a Ag wire quasi-reference electrode. Scan rates from 20 to 5000 mV/s were employed in the cyclic voltammetry scans to assess the chemical and electrochemical reversibility of the observed redox transformations. Half-wave potentials were determined from the peak values in the square-wave voltammograms or from the average of the cathodic and anodic peak potentials in the reversible cyclic voltammograms. Potential calibrations were performed at the end of each data collection cycle using the ferrocenium/ferrocene couple as an internal standard. Electronic absorption and cyclic voltammetric data were analyzed using Wavemetrics IGOR Pro (version 6.04) software on a Macintosh platform.

Magnetic Susceptibility. Magnetic susceptibility data were collected using a Quantum Design Superconducting Quantum Interference Device (SQUID) magnetometer at 6.5 T from 2 to 400 K. The samples were sealed in a 5 mm Wilmad 505-PS NMR tube along with a small amount of quartz wool, which held the sample near the tube center. Contributions to the magnetization from quartz wool and the NMR tube were measured independently and subtracted from the total measured signal. Diamagnetic corrections were made with the use of Pascal's constants. Measurements on samples of fresh batches of the compound were duplicated to ensure veracity of the results.

Crystallography. Crystals were mounted in a nylon cryoloop using Paratone-N oil under an argon gas flow. The data were collected on a Bruker D8 APEX II charge-coupled-device diffractometer, with a KRYO-FLEX liquid nitrogen vapor cooling device. The instrument was equipped with graphite monochromatized Mo Kα X-ray source (λ = 0.71073 Å), with MonoCap X-ray source optics. Hemispheres of data were collected using ω scans. Data collection and initial indexing and cell refinement were handled using APEX II software.[64] Frame integration, including Lorentz-polarization corrections, and final cell parameter calculations were carried out using SAINT+ software.[65] The data were corrected for absorption using the SADABS program.[66] Decay of the reflection intensity was monitored by analysis of the redundant frames. The structure was solved using direct methods and difference Fourier techniques. Unless otherwise noted, non-hydrogen atoms were refined anisotropically and hydrogen atoms were treated as idealized contributions. Residual electron density originating from solvent contributions was removed using SQUEEZE/PLATON.[67] Structure solution, refinement, graphics, and creation of the publication materials were performed using SHELXTL.[68]

Acknowledgment. For financial support of this work, we acknowledge the Division of Chemical Sciences, Office of Basic Energy Sciences, Heavy Element Chemistry program, LANL (Director's and Frederick Reines PD Fellowships), the LANL G. T. Seaborg Institute for Transactinium Science, and the LANL Laboratory Directed Research & Development program. Finally, we thank Drs. Stosh A. Kozimor and Rebecca M. Chamberlin (LANL) for helpful discussions.

Supporting Information Available: Crystallographic information in CIF format; electrochemical data for complexes **1**, **1-THF**, and **2-THF**; variable THF concentration UV−vis absorption spectra for isosbestic point determination for **1**; tables presenting the full orbital populations for complexes **1** and **1-THF** and a comparison of the U−N bond distances obtained for experimental and calculated structures of complexes **1** and **1-THF**; and full output for the ground state and first excited state CASSCF calculations of **1-THF**. This material is available free of charge via the Internet at http://pubs.acs.org.

(59) Becke, A. D. *J. Chem. Phys.* **1993**, *98*, 5648–5652.
(60) Küchle, W.; Dolg, M.; Stoll, H.; Preuss, H. *J. Chem. Phys.* **1994**, *100*, 7535–7542.
(61) Fuentealba, P.; Preuss, H.; Stoll, H.; Szentpaly, L. v. *Chem. Phys. Lett.* **1982**, *89*, 418–422.
(62) Küchle, W.; Dolg, M.; Stoll, H.; Preuss, H. *Mol. Phys.* **1991**, *74*, 1245–1263.
(63) Frisch, M. J. *Gaussian03*; Gaussian, Inc.: Wallingford, CT, 2004.
(64) *APEX II*; Bruker Analytical X-Ray Systems, Inc.: Madison, WI, 1997.
(65) *SAINT 7.03*; Bruker Analytical X-Ray Systems, Inc.: Madison, WI, 2003.
(66) Sheldrick, G. M. *SADABS 2.03*; University of Göttingen: Göttingen, Germany, 2001.
(67) Spek, A. L. *PLATON*; Utrecht University: Utrecht, The Netherlands, 2005.
(68) Sheldrick, G. M. *SHELXTL 5.10*; Bruker Analytical X-Ray Systems, Inc.: Madison, WI, 1997.